

Holographic Evolution with Dynamical Boundary Gravity

Christian Ecker,¹ Wilke van der Schee,² David Mateos,^{3,4} and Jorge Casalderrey-Solana³

¹*Institut für Theoretische Physik, Goethe Universität,
Max-von-Laue-Str. 1, 60438 Frankfurt am Main, Germany*

²*Theoretical Physics Department, CERN, CH-1211 Genève 23, Switzerland*

³*Departament de Física Quàntica i Astrofísica & Institut de Ciències del Cosmos (ICC),
Universitat de Barcelona, Martí i Franquès 1, 08028 Barcelona, Spain*

⁴*Institució Catalana de Recerca i Estudis Avançats (ICREA), Lluís Companys 23, Barcelona, Spain*

Holography has provided valuable insights into the time evolution of strongly coupled gauge theories in a fixed spacetime. However, this framework is insufficient if this spacetime is dynamical. We present a novel scheme to evolve a four-dimensional, strongly interacting gauge theory coupled to four-dimensional dynamical gravity in the semiclassical regime. We use holography to evolve the quantum gauge theory stress tensor. The four-dimensional metric evolves according to the four-dimensional Einstein equations coupled to the expectation value of the stress tensor. We focus on Friedmann-Lemaître-Robertson-Walker geometries and evolve far-from-equilibrium initial states that lead to asymptotically expanding, flat or collapsing Universes.

Keywords: gauge/gravity duality, QFT on curved background, cosmology, hydrodynamics

1. Introduction. Holography relates the quantum-mechanical time evolution of a strongly coupled, four-dimensional (4D) gauge theory to that of classical gravity in a five-dimensional (5D) asymptotically anti de Sitter (AAdS) spacetime. The power of this correspondence is that it allows the use of classical gravity in 5D to tackle otherwise intractable problems on the gauge theory side.

The spacetime where the gauge theory is formulated is identified with the boundary of AAdS. We will refer to its 4D metric as the “boundary metric”, and to the 5D metric in AAdS as the “bulk metric”. In many applications of holography the boundary metric is taken to be non-dynamical. For example, this metric is flat in the holographic description of the quark-gluon plasma [1, 2] or in applications to condensed matter systems [3–5]. Applications with a curved metric include gauge dynamics in black hole backgrounds [6] or in de Sitter (dS) space [7–12]. In all these cases the boundary metric influences, but is unaffected by, the gauge theory dynamics. In other words, the backreaction of the gauge degrees of freedom on the metric is not included.

Despite its successes, this framework is insufficient if the boundary metric is dynamical. This limits potential applications of holography to cosmological defects, phase transitions in the early Universe, neutron star mergers, inflation, pre- or re-heating, cosmological instabilities, etc. The purpose of this letter is to present a scheme capable of evolving a strongly interacting 4D gauge theory coupled to 4D dynamical gravity.

We are interested in the semiclassical gravity regime in which the gauge theory is quantum mechanical but the metric obeys the classical Einstein equations sourced by the expectation value of the gauge theory stress tensor:

$$R_{\mu\nu} - \frac{1}{2}Rg_{\mu\nu} + \Lambda g_{\mu\nu} = 8\pi G \langle T_{\mu\nu} \rangle. \quad (1)$$

All quantities in this equation, including Newton’s con-

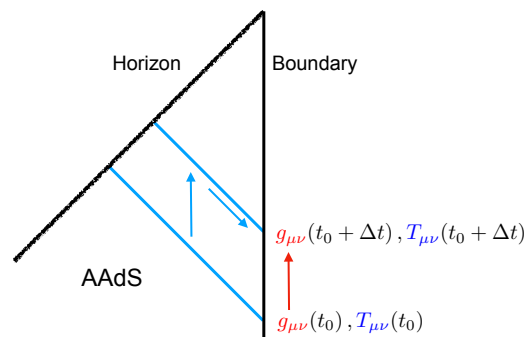


FIG. 1. Penrose diagram of our evolution scheme. The diagonal blue lines are four-dimensional null slices in the bulk. Each point on the vertical black line is a three-dimensional spatial slice of the boundary spacetime.

stant G and a possible cosmological constant Λ , refer to the 4D boundary theory. Hereafter we will refer to the gauge theory stress tensor simply as “the stress tensor”. Since this is $\mathcal{O}(N^2)$ in the large- N limit, we assume that G is $\mathcal{O}(N^{-2})$ in order to have a finite backreaction. In the following we work with N -independent quantities defined via the rescalings $T_{\mu\nu} \rightarrow (2\pi^2/N^2) T_{\mu\nu}$ and $G \rightarrow (N^2/2\pi^2) G$.

The key point in the semiclassical regime is to determine the quantum-mechanical evolution of the stress tensor, which must be done self-consistently in the presence of the dynamical metric $g_{\mu\nu}$. We use holography to determine this evolution (see Fig. 1). The initial state at time t_0 is defined by the 5D fields on a bulk null slice, together with the 4D metric on a boundary spatial slice. These two sets of initial data must satisfy non-trivial “corner” consistency conditions that we will analyse below (see [13–16] for related discussions). For the moment, it suffices to say that the leading term in the near-boundary fall-off of the bulk metric must coincide with the bound-

ary metric, whereas the subleading term in this fall-off determines the expectation value of the stress tensor. To evolve to a time $t' = t_0 + \Delta t$, we first use equation (1) to determine the new boundary metric at t' . Because AAdS is not globally hyperbolic, this new metric provides necessary boundary conditions that allow us to evolve the 5D bulk equations to determine the new bulk fields at t' . The subleading term of the 5D metric near the boundary then determines the stress tensor at t' .

Our scheme amounts to imposing mixed boundary conditions on the five-dimensional fields [17]. Our strategy differs from previous work in essential ways. We do not introduce an ultraviolet cut-off in the gauge theory or branes in the bulk [18–26] but work directly with dynamical gravity at the boundary. As a consequence, we have complete freedom to choose the dynamical equations obeyed by the boundary metric. We do not make use of predetermined bulk solutions [27–29] or restrict ourselves to constant-curvature boundary metrics [30], but instead construct both the bulk and the boundary geometries dynamically, one time step at a time. We do not assume a perfect-fluid form for the stress tensor [31] but allow for arbitrarily-far-from-equilibrium dynamics. Our full code is publicly available [32].

2. Model and scheme. We use the same model as in [12]. The 5D bulk theory consists of gravity coupled to a scalar field ϕ . The 4D gauge theory is a large- N , strongly coupled, non-conformal theory with a mass scale M . We measure all dimensionful quantities in units of M . For simplicity, we focus on homogeneous and isotropic states in the 4D theory, namely on Friedmann-Lemaître-Robertson-Walker cosmologies. As a consequence, the boundary metric is completely determined by a scale factor $a(t)$, and the only non-zero components of the stress tensor are the energy density $\mathcal{E}(t)$ and the pressure $\mathcal{P}(t)$. Under these conditions, (1) reduces to the Friedmann equation

$$\left(\frac{\dot{a}}{a}\right)^2 \equiv H^2 = \frac{1}{3} \Lambda + \frac{8\pi G}{3} \mathcal{E} \quad (2)$$

and the continuity equation

$$\dot{\mathcal{E}} = -3H(\mathcal{E} + \mathcal{P}), \quad (3)$$

with $H = \dot{a}/a$ the Hubble rate.

The holographic determination of the stress tensor requires renormalization of the bulk gravitational action [33, 34]. This entails the addition of appropriate counterterms. The coefficients of some counterterms are fixed by the requirement that they cancel divergences in the bulk action, whereas those of finite counterterms can be chosen arbitrarily. This corresponds to the freedom in the choice of scheme in the gauge theory. The contribution of the finite counterterms to the stress tensor amounts to a renormalization of the bare values of G and Λ in (1)

[29], as well as of the bare coefficients of possible higher-derivative curvature terms that were omitted in (1). We choose the gauge theory scheme as follows. First, we set $\alpha = 0, \beta = 1/16$ for the coefficients in [12]. With this choice the stress tensor in flat space vanishes, and the constants G and Λ in (1) are directly the effective ones. Second, consistently with the semiclassical regime, we set to zero the effective values of all the possible higher-derivative terms in (1).

Having fixed the scheme, below we will extract the stress tensor from the near-boundary fall-off of the 5D fields. For illustration, consider the bulk scalar field. In an appropriate null holographic coordinate r with the boundary at $r \rightarrow \infty$ we have [12]

$$\phi = \frac{M}{r} + \frac{\phi_2(t)}{r^3} + \frac{1}{r} \sum_{n \geq 3} \frac{\phi_n(t)}{r^n} + \frac{1}{r} \sum_{n \geq 2} \frac{\psi_n(t) \log r}{r^n} + \dots \quad (4)$$

The logarithmic terms are specific to odd-dimensional bulk spacetimes [35]. The near-boundary analysis only leaves undetermined $\phi_2(t)$. The remaining coefficients $\phi_{n \geq 3}$ and $\psi_{n \geq 2}$ are given in terms of $\phi_2(t)$, $a(t)$ and their derivatives by expressions of the form

$$\phi_n \left(M, a, \dot{a}, \dots, a^{(n)}, \phi_2, \dot{\phi}_2, \dots, \phi_2^{(n-2)} \right), \quad (5a)$$

$$\psi_n \left(M, a, \dot{a}, \dots, a^{(n)} \right). \quad (5b)$$

There is a similar expression for the fall-off of the 5D bulk metric with one undetermined coefficient $a_4(t)$. From the bulk viewpoint, the function $\phi(r, t_0)$ and the coefficient $a_4(t_0)$ at an initial time t_0 are free data. Moreover, if this data and the scale factor $a(t_0)$ are known, then integration of the constraints coming from the Einstein-scalar equations in the bulk determines the entire 5D metric on the initial time slice at $t = t_0$.

Eqs. (5), which arise from the bulk equations of motion, constitute a set of constraints that relate the bulk initial condition $\phi(r, t_0)$ and the derivatives of the boundary scale factor. These corner conditions imply that the initial data on the bulk slice and the boundary conditions on that slice cannot be specified independently. For a non-dynamical boundary metric, as is in e.g. [36], $a(t)$ can be prescribed arbitrarily and these bulk constraints can be used to determine the $\psi_n(t)$ coefficients. In contrast, in the case of dynamical boundary gravity, it is highly non-trivial that these bulk constraints can be made compatible with those coming from the boundary Einstein equations (1). The latter arise as follows. The stress tensor depends on the undetermined coefficients and on the scale factor via expressions of the form [12]

$$\mathcal{E}(a_4, \phi_2, a, \dot{a}, \ddot{a}), \quad \mathcal{P}(a_4, \phi_2, a, \dot{a}, \ddot{a}). \quad (6)$$

These, together with (2), (3) and (5a), can be shown to determine all the derivatives of the scale factor at t_0 in terms of $a(t_0)$, $a_4(t_0)$ and $\phi_n(t_0)$. Through

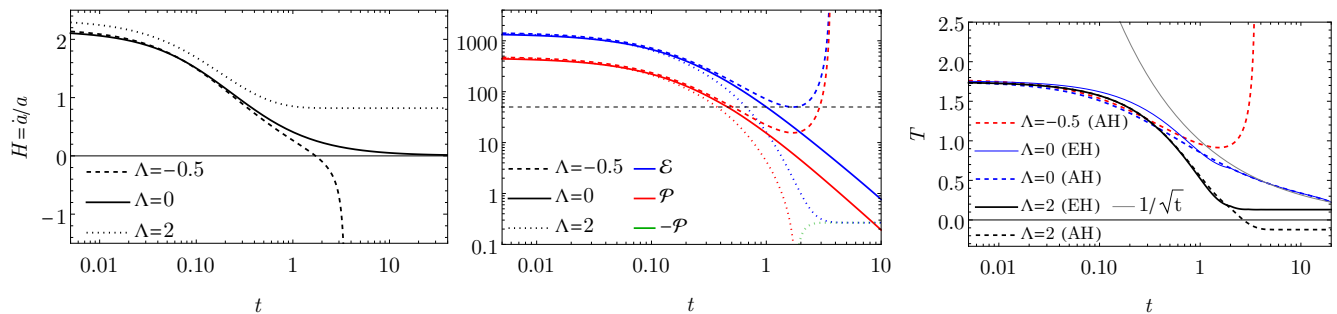


FIG. 2. Evolution of the Hubble rate (left), of the energy density and pressure (center), and of the effective temperature (right), for $G = 1/2500$ and three different values of Λ .

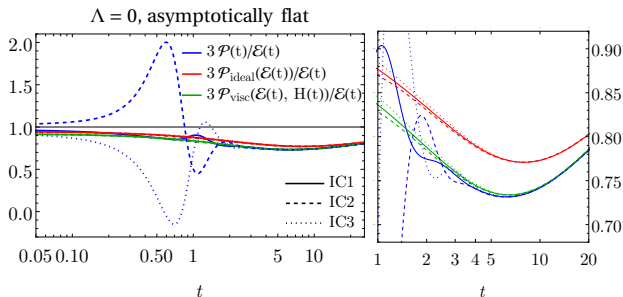


FIG. 3. Comparison between the holographic result for the pressure/energy ratio (blue) and the ideal (red) and viscous (green) hydrodynamic approximations, for $G = 1/750$, $\Lambda = 0$ and three different initial conditions.

(5b), this fixes all the logarithmic terms in $\phi(r, t_0)$. This is particularly important for our scheme because numerically we work with “subtracted” variables that differ from the original ones by a number of logarithmic (and some non-logarithmic) terms. Specifically, our evolution scheme is as follows. At t_0 we specify $a(t_0)$, $a_4(t_0)$, $\phi_2(t_0)$ and the subtracted version of $\phi(r, t_0)$. We then use the procedure above to find $a^{(n)}(t_0)$ up to $n = 4$. These determine all the necessary logarithmic terms. Next we integrate the Einstein-scalar constraints and find all the bulk data on the initial time slice. By construction this is consistent with the corner conditions up to the desired order. Finally, we use the bulk and the boundary evolution equations to obtain a , a_4 , ϕ_2 and the subtracted version of ϕ at $t_0 + \Delta t$.

3. Results. We perform evolutions for three different values of the cosmological constant $\Lambda = \{-0.5, 0, 2\}$. As initial data at $t_0 = 0$ we use $a(0) = 1$ and a radial profile $\phi(r, t_0)$ that corresponds to a thermal equilibrium state in flat space. In all cases we choose $a_4(0) = -2000$, except in Fig. 3, for which $a_4(0) = -100$.

Fig. 2(left) shows the evolution of the Hubble rate. Negative Λ leads to a “Big Crunch” where the Hubble rate evolves towards minus infinity and the spacetime collapses. For $\Lambda = 0$ the Hubble rate decays to zero and

the spacetime approaches Minkowski space. Positive Λ leads to an exponentially expanding dS Universe.

Fig. 2(center) shows \mathcal{E} and \mathcal{P} . For $\Lambda < 0$ the energy density reaches a minimum, after which it diverges as the Big Crunch is approached. For $\Lambda = 0$, \mathcal{E} and \mathcal{P} decrease in a power-law fashion that is well described by hydrodynamics (see below). For $\Lambda > 0$ the Universe approaches dS with a small Casimir contribution from the non-conformal matter, $\mathcal{E}_{\text{dS}} = -\mathcal{P}_{\text{dS}} \approx 0.2667$ [37].

In Fig. 2(right) we show the temperature of the gauge theory state, $T = \kappa/2\pi$, computed from the surface gravity, κ , of the event (EH) and of the apparent (AH) horizons of the bulk geometry. For $\Lambda < 0$ the AH reaches the boundary of AAdS at a finite boundary proper time. The boundary itself collapses at this point, and T_{AH} diverges. We do not show T_{EH} because the definition of the EH is unclear in this case. For $\Lambda > 0$ the temperatures at late times approach $T_{\text{EH}} = -T_{\text{AH}} = H/2\pi$, in agreement with [9, 12]. For $\Lambda = 0$ the horizon falls deep into the bulk and at late times $H \propto t^{-1}$ and $T \propto t^{-1/2}$, as expected. In addition, Eqn. (2) implies $\mathcal{E}/H^4 \sim t^2/G \gg 1$, meaning that the dynamics is dominated by the energy density. As a consequence, the late-time boundary state approaches a thermal state in Minkowski space and the bulk EH and AH become indistinguishable.

Holography can evolve strongly-coupled, far-from-equilibrium, quantum matter which, after some time, is expected to enter a hydrodynamic regime (except in dS [12], see below). For $\Lambda = 0$ this is illustrated in Fig. 3, which shows the evolution of the pressure/energy ratio for three different initial conditions, IC1, IC2 and IC3. For IC2 and IC3 we added respectively $+2$ and -1.5 to the subtracted $\phi(r, 0)$ of IC1. This leads to evolutions that are just about numerically stable and hence as far from equilibrium as our code allows. The blue curves are the holographic results. The difference with the viscous hydrodynamic approximation [12] (green curves) at early times shows that the initial dynamics is far from equilibrium. After $\Delta t \approx 2$ the evolution becomes well described by viscous hydrodynamics, consistently with a hydrodynamization time of $\mathcal{O}(1/T)$ [38, 39]. The comparison to

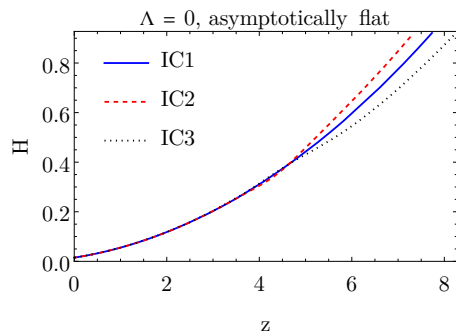


FIG. 4. Evolution of the Hubble rate as function of redshift z for the three different initial conditions presented in Fig. 3.

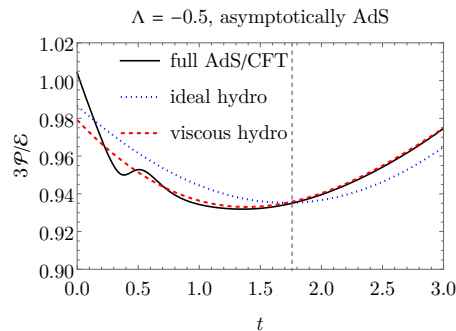


FIG. 5. Comparison between the holographic result for the pressure/energy ratio (black) and the ideal (blue) and viscous (red) approximations, for $G = 1/2500$ and $\Lambda = -0.5$.

ideal hydrodynamics in the right panel of Fig. 3 shows that viscous corrections can be sizable even at late times.

The initial far-from-equilibrium period leaves an imprint on the scale factor. This is illustrated in Fig. 4, which shows the Hubble rate for the three evolutions of Fig. 3 as a function of the redshift $z(t) = a(t_{\text{obs}})/a(t) - 1$. The time t_{obs} is defined for each curve by the physical condition that \mathcal{E} reaches some late-time value, in this case $\mathcal{E}(t_{\text{obs}}) = 0.02$. At small redshift the evolutions are equivalent as a consequence of the applicability of hydrodynamics at late times shown in Fig. 3. In contrast, at large redshift the far-from-equilibrium dynamics at early times leads to significantly different Hubble rates.

In Fig. 5 we show the analogous results for $\Lambda = -0.5$. The dashed, grey line marks the time where \mathcal{E} reaches a minimum and $H = 0$. The entire evolution is well described by viscous hydrodynamics. As above, viscous corrections are non-negligible at late times.

Fig. 6 illustrates the asymptotically dS case. At late times the backreaction is dominated by the cosmological constant, which here includes a Casimir contribution that we subtract in the plot. Once the expansion has diluted the energy density so that $\mathcal{E} - \mathcal{E}_{\text{dS}} \lesssim H^4$, the system is driven out of equilibrium and the hydrodynamic approximation ceases to be valid, as expected from the

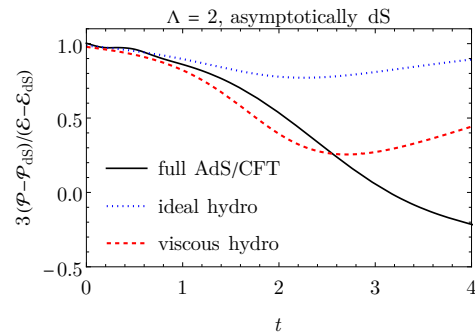


FIG. 6. Same as in Fig. 5 but for $\Lambda = 2$.

non-backreacted analysis [12].

4. Discussion. We have provided the first example of holographic time evolution with dynamical boundary gravity in which both the bulk and the boundary geometries are constructed dynamically, one time step at a time. In order to illustrate our approach in the simplest possible setting, we have focused on homogeneous and isotropic states. However, we expect that our scheme can be generalised to situations with no symmetry assumptions. Our work should thus be viewed as a proof of concept that opens the door to new applications of holography that we will develop elsewhere. Here we just close with brief comments on two of them.

Inflation could be studied by promoting the boundary value of the bulk scalar field to a dynamical boundary scalar field which would play the role of the inflaton. This would allow us to use holography to study e.g. the pre- and re-heating processes at the end of inflation [40, 41].

In the absence of symmetry assumptions, cosmological backgrounds are expected to suffer from instabilities [42]. This has been studied holographically in the linear approximation [11]. Our approach would allow us to determine the endpoint of these instabilities deep into the nonlinear regime.

Acknowledgements. We thank R. Emparan, G. Horowitz, E. Kiritsis and J. Mas for discussions. JCS and DM are supported by grants SGR-2017-754, PID2019-105614GB-C21, PID2019-105614GB-C22 and the “Unit of Excellence MdM 2020-2023” award to the Institute of Cosmos Sciences (CEX2019-000918-M).

-
- [1] J. Casalderrey-Solana, H. Liu, D. Mateos, K. Rajagopal, and U. A. Wiedemann, *Gauge/String Duality, Hot QCD and Heavy Ion Collisions* (Cambridge University Press, 2014) [arXiv:1101.0618 \[hep-th\]](#).
 - [2] W. Busza, K. Rajagopal, and W. van der Schee, *Ann. Rev. Nucl. Part. Sci.* **68**, 339 (2018), [arXiv:1802.04801 \[hep-ph\]](#).
 - [3] J. Zaanen, Y.-W. Sun, Y. Liu, and K. Schalm, *Holo-*

- graphic Duality in Condensed Matter Physics* (Cambridge Univ. Press, 2015).
- [4] S. A. Hartnoll, A. Lucas, and S. Sachdev, (2016), [arXiv:1612.07324 \[hep-th\]](#).
- [5] H. Nastase, *String Theory Methods for Condensed Matter Physics* (Cambridge University Press, 2017).
- [6] D. Marolf, M. Rangamani, and T. Wiseman, *Class. Quant. Grav.* **31**, 063001 (2014), [arXiv:1312.0612 \[hep-th\]](#).
- [7] J. Maldacena and G. L. Pimentel, *JHEP* **02**, 038 (2013), [arXiv:1210.7244 \[hep-th\]](#).
- [8] W. Fischler, S. Kundu, and J. F. Pedraza, *JHEP* **07**, 021 (2014), [arXiv:1311.5519 \[hep-th\]](#).
- [9] A. Buchel and A. Karapetyan, *JHEP* **03**, 114 (2017), [arXiv:1702.01320 \[hep-th\]](#).
- [10] A. Buchel, M. P. Heller, and J. Noronha, *Phys. Rev. D* **94**, 106011 (2016), [arXiv:1603.05344 \[hep-th\]](#).
- [11] P. M. Chesler and A. Loeb, *JCAP* **11**, 010 (2020), [arXiv:2003.05501 \[hep-th\]](#).
- [12] J. Casalderrey-Solana, C. Ecker, D. Mateos, and W. Van Der Schee, *JHEP* **03**, 181 (2021), [arXiv:2011.08194 \[hep-th\]](#).
- [13] H. Friedrich, *J. Geom. Phys.* **17**, 125 (1995).
- [14] A. Enciso and N. Kamran, *J. Diff. Geom.* **112**, 505 (2019), [arXiv:1412.4376 \[math.AP\]](#).
- [15] D. A. Carranza and J. A. Valiente Kroon, *Class. Quant. Grav.* **35**, 245006 (2018), [arXiv:1807.04212 \[gr-qc\]](#).
- [16] G. T. Horowitz and D. Wang, *JHEP* **01**, 155 (2020), [arXiv:1909.11703 \[hep-th\]](#).
- [17] G. Compere and D. Marolf, *Class. Quant. Grav.* **25**, 195014 (2008), [arXiv:0805.1902 \[hep-th\]](#).
- [18] C. Csaki, M. Graesser, C. F. Kolda, and J. Terning, *Phys. Lett. B* **462**, 34 (1999), [arXiv:hep-ph/9906513](#).
- [19] A. Kehagias and E. Kiritsis, *JHEP* **11**, 022 (1999), [arXiv:hep-th/9910174](#).
- [20] J. M. Cline, C. Grojean, and G. Servant, *Phys. Rev. Lett.* **83**, 4245 (1999), [arXiv:hep-ph/9906523](#).
- [21] C. Csaki, M. Graesser, L. Randall, and J. Terning, *Phys. Rev. D* **62**, 045015 (2000), [arXiv:hep-ph/9911406](#).
- [22] G. R. Dvali, G. Gabadadze, and M. Porrati, *Phys. Lett. B* **484**, 112 (2000), [arXiv:hep-th/0002190](#).
- [23] A. Karch and L. Randall, *JHEP* **05**, 008 (2001), [arXiv:hep-th/0011156](#).
- [24] E. Kiritsis, *JCAP* **10**, 014 (2005), [arXiv:hep-th/0504219](#).
- [25] X. Dong, B. Horn, S. Matsuura, E. Silverstein, and G. Torroba, *Phys. Rev. D* **85**, 104035 (2012), [arXiv:1108.5732 \[hep-th\]](#).
- [26] R. Emparan, A. M. Frassino, and B. Way, *JHEP* **11**, 137 (2020), [arXiv:2007.15999 \[hep-th\]](#).
- [27] P. S. Apostolopoulos, G. Siopsis, and N. Tetradis, *Phys. Rev. Lett.* **102**, 151301 (2009), [arXiv:0809.3505 \[hep-th\]](#).
- [28] J. Erdmenger, K. Ghoroku, and R. Meyer, *Phys. Rev. D* **84**, 026004 (2011), [arXiv:1105.1776 \[hep-th\]](#).
- [29] S. Banerjee, S. Bhowmick, A. Sahay, and G. Siopsis, *Class. Quant. Grav.* **30**, 075022 (2013), [arXiv:1207.2983 \[hep-th\]](#).
- [30] J. K. Ghosh, E. Kiritsis, F. Nitti, and L. T. Witkowski, *JCAP* **07**, 040 (2020), [arXiv:2003.09435 \[hep-th\]](#).
- [31] S. Fischetti, D. Kastor, and J. Traschen, *Class. Quant. Grav.* **31**, 235007 (2014), [arXiv:1407.4299 \[hep-th\]](#).
- [32] <http://wilkevanderschee.nl/public-codes>.
- [33] M. Henningson and K. Skenderis, *JHEP* **07**, 023 (1998), [arXiv:hep-th/9806087](#).
- [34] S. de Haro, S. N. Solodukhin, and K. Skenderis, *Commun. Math. Phys.* **217**, 595 (2001), [arXiv:hep-th/0002230](#).
- [35] C. Fefferman and C. R. Graham, in *Élie Cartan et les mathématiques d'aujourd'hui - Lyon, 25-29 juin 1984*, Astérisque No. S131 (Société mathématique de France, 1985).
- [36] P. M. Chesler and L. G. Yaffe, *Phys. Rev. Lett.* **102**, 211601 (2009), [arXiv:0812.2053 \[hep-th\]](#).
- [37] This value is consistent with [12] after taking into account a typo in Sec 4.3 of [12], where we wrote that we chose $\alpha = 0$ while the actual value was $\alpha = 3/4$.
- [38] M. P. Heller, R. A. Janik, and P. Witaszczyk, *Phys. Rev. Lett.* **108**, 201602 (2012), [arXiv:1103.3452 \[hep-th\]](#).
- [39] M. P. Heller, D. Mateos, W. van der Schee, and D. Trancanelli, *Phys. Rev. Lett.* **108**, 191601 (2012), [arXiv:1202.0981 \[hep-th\]](#).
- [40] L. Kofman, A. D. Linde, and A. A. Starobinsky, *Phys. Rev. Lett.* **73**, 3195 (1994), [arXiv:hep-th/9405187](#).
- [41] L. Kofman, A. D. Linde, and A. A. Starobinsky, *Phys. Rev. D* **56**, 3258 (1997), [arXiv:hep-ph/9704452](#).
- [42] V. F. Mukhanov, L. R. W. Abramo, and R. H. Brandenberger, *Phys. Rev. Lett.* **78**, 1624 (1997), [arXiv:gr-qc/9609026](#).